J Mater Sci (2011) 46:6690–6699
DOI 10.1007/s10853-011-5622-5

Effects of current intensity and cumulative exposure time on the localized current-activated sintering of titanium nickelides

M. Patel · K. S. Moon · S. K. Kassegne · K. Morsi

Received: 13 February 2011 / Accepted: 9 May 2011 / Published online: 26 May 2011

Abstract This article discusses the processing and properties of titanium nickelides locally sintered via Current-Activated Tip-based Sintering (CATS), a new localized sintering process. One of the advantages of CATS is the ability to apply orders of magnitude higher current densities than conventionally possible, which can promote rapid sintering and phase transformation rates. Mechanically alloyed equi-atomic Ni–Ti powder was for the first time tip sintered at varying current intensities and cumulative current exposure time. The effect of current-control processing conditions on the evolution of the locally sintered Ni–Ti microstructure and properties are discussed. The size of the locally sintered process zone was found to increase with cumulative current exposure time. The degree of sintering, phase transformations, and properties were found to depend on the current intensity, cumulative current exposure time and distance away from the tip/compact interface. Fully/near fully dense material was achieved rapidly at locations exposed to the highest current densities.

Introduction

Titanium nickelides have received a great deal of attention over the past few decades, with research efforts expended in the understanding of their mechanical properties, electrical properties, phase transformations, shape memory properties, and processing [1, 2]. Although numerous traditional manufacturing processes have been used to produce titanium nickelides such as casting [3] and thermomechanical processing [4, 5], powder-based processing has emerged as an approach that can yield significant benefits which include net shape processing, reduced material waste, and microstructural and compositional controls. These materials can be produced cost effectively from elemental powders of Ti and Ni which can react exothermically to form and reactively sinter the intermetallic simultaneously [6], from pre-alloyed powder obtained, for example, via the mechanical alloying (MA) process [7], or atomization [8]. Such powders have previously been consolidated using different approaches which include pressure-less sintering [9], hot isostatic pressing [10], and recently using spark plasma sintering (SPS) [11, 12, 31].

SPS has the advantage of achieving sintering at considerably less temperatures and times than conventionally possible [13, 14], leading to further advantages in terms of grain size retention which is especially relevant for nanostructured materials. In the basic configuration of SPS, powders are placed in a graphite die and pressed while passing pulsed electric current that heats the compact to the sintering temperature. While the process offers many advantages, it is limited to the production of macro-scale artifacts of predominantly simple geometries. Moreover, many SPS studies have inadvertently ignored the role of electric current as a dominant processing parameter and only report temperature during processing, despite clear evidence of the intrinsic role of electric current in enhancement of sintering in SPS [13]. With the increasing interest in the use of titanium nickelides as micro-actuators and sensors [15, 16], it is imperative to explore new

M. Patel · K. S. Moon · S. K. Kassegne · K. Morsi (✉)
Department of Mechanical Engineering, San Diego State University (SDSU), 5500 Campanile Drive, San Diego, CA 92182, USA
e-mail: Kmorsi@Mail.Sdsu.Edu

powder-based processing approaches to enable such products, while avoiding the cost and process complexities of other processes such as lithography. Powder injection molding of titanium nickelides has also been previously investigated [17]; however, it involves multiple steps of powder pre-alloying, binder/wax/powder mixing, injection molding, de-waxing followed by thermal de-binding and then sintering.

As an alternative method, three of the authors have recently developed a new process [Current-activated Tip-based Sintering (CATS)] which uses either a stationary or moving small conducting tip to locally sinter powder compacts/beds to produce unconventionally small sintered material [18]. The tip can be macro-, micro-, or even nano-scale, and is 'precision-controlled in terms of displacement, speed, and applied pressure. Advantages of this recently patented process [19] over SPS include the ability to apply orders of magnitude higher current densities due to the small tip size (while using minimal input energy), which in turn can facilitate exceedingly rapid sintering rates. The experimental configuration in CATS inherently differs from that of SPS, for example, the absence of a conventional die material (i.e., graphite). Instead of a conventional die, in CATS, the powder/compact surrounds the locally sintered/sintering region (i.e., the process zone under the tip) which itself is constantly evolving during sintering. Hence, the local heat transfer characteristics is unique, giving rise to current and temperature distributions within the vicinity of the tip that play a major role in the localized sintering behavior. Initial study, with limited variations in process parameters, was conducted on ultra-fine elemental nickel powder proving the feasibility of this approach in localizing the current-assisted sintering in small regions of a powder compact [18]. Recently, research has been published by Locci et al. [20] on the field-activated, pressure-assisted sintering of NiTi, in which *reactive* powder mixes of elemental Ti and Ni where reactively sintered under varying alternating current densities up to 0.53 kA/cm^2. To the best of the authors' knowledge, there has been no previous study that investigated the effect of "direct, DC" electric current exposure or intensity on the evolution of 'pre-alloyed' Ni/Ti powder body/compact (which excludes the reactive "exothermic" component) during SPS or CATS, not to mention under high current densities. In this study, CATS of mechanically alloyed Ni–Ti powder is presented for the first time, with special attention to electric current intensity as a processing variable up to unprecedented nominal current densities of 12.7 kA/cm^2. A detailed investigation of the effect of CATS processing parameters on the evolution of the local microstructure in terms of degree of sintering, phase transformations, and properties has been carried out and discussed.

Experimental procedures

Titanium powder (−200 mesh, 99.7% Purity, Atlantic Equipment Engineers, USA) and nickel powder (−170/+325 mesh, 99.9% purity, from Atlantic Equipment Engineers, USA) were used in the study. Figure 1 shows the size and morphology of the starting nickel and titanium powders which are spherical/rounded and angular, respectively.

Nickel and titanium powders were mixed at 50/50 atomic percent and ball milled (using steel balls) for up to 10 h in 30-min intervals with a 10-min rest following each milling interval (to avoid heat build-up), using a ball-to-powder weight ratio of 10:1. The mechanically alloyed powder was characterized to ascertain the condition of the powder before performing CATS. During the MA process [21], powders are impacted by the milling balls, which deform the particles, causing work hardening, followed by fracture and particle re-welding. The continuation of this process leads to the homogenous atomic mixing of the powders. The median particle size of the Ni–Ti alloyed powders was found to first increase with milling time followed by a decrease, with powders milled for 10 h having D_{10}, D_{50}, and D_{90} of 20.3, 34.6, and 60.5 μm, respectively. This is in good agreement with particle size development in the MA process [22], where work hardening and fracture (leading to particle size reduction) overrides particle re-welding events (which promotes particle size increase). It is important to mention that in contrast to previous study [7] that reported low powder yields following the MA of Ni–Ti (due to powder sticking to containers/balls), we were successful in producing 100% yield (i.e., all powder mass originally placed inside the milling vial was recovered). This was achieved by leaving the milling vial to cool at the end of the milling period, then milling for an extra 1–2 min, before opening the milling vial to remove all the powder.

The 10-h-milled powder was subsequently uni-axially pressed in a hardened steel die to produce green compacts of dimensions of 14.2-mm diameter and ~2.8-mm thickness, and a green density of ~4.2 g/cm^3. CATS was performed on the surface of each of the green compacts using a stationary tungsten tip of material-contacting diameter 1 mm positioned centrally on the powder compact while maintaining contact via a flexural loading arrangement (Fig. 2 shows the experimental setup). Direct electric current intensity up to 100 A (equivalent to a nominal current density of ~12.7 A/cm^2) at 2–5 V was applied to the contact surface through the tungsten tip in the form of duty cycles. Each duty cycle comprises 1 s on and 11 s off up to 100 cycles, with the use of direct current only. This cycling is in contrast to the typical pulses used in SPS, where the on–off is in milliseconds [23, 31]. Here, the purpose of the

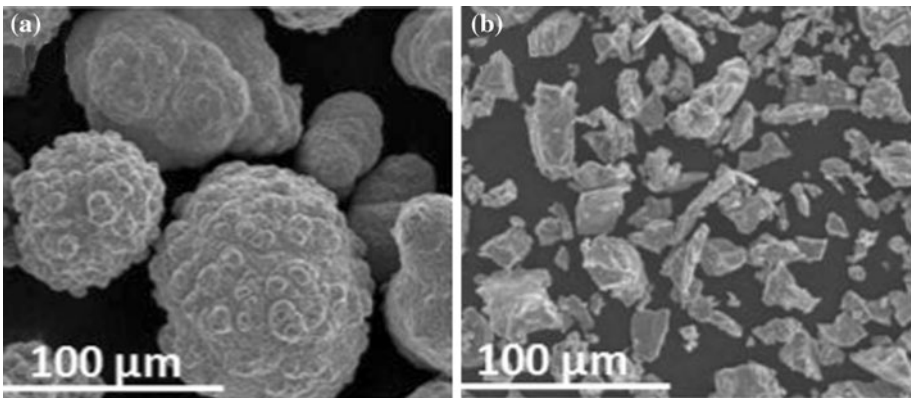

Fig. 1 **a** Ni and **b** Ti as-received powders used in the investigation

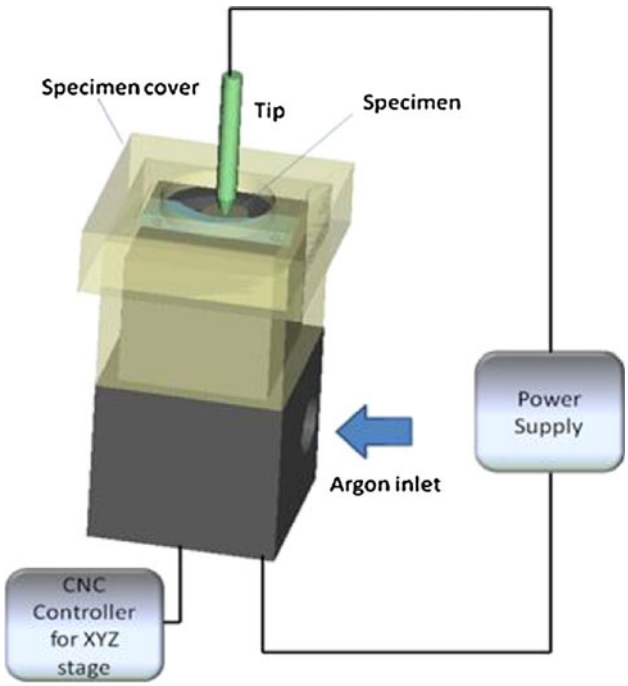

Fig. 2 Model of the CATS setup used in the present investigation, using a micro-CNC (computer numerical control)

cycling is to confine the heating to the region beneath the tip, and reduce heat transfer to the remaining compact, thus aiding localization.

For powder characterization, X-ray diffraction (XRD) and scanning electron microscopy (SEM) were performed on the mechanically alloyed powders. For micro-structural characterization, sintered samples were cross sectioned centrally across the depth and polished to 1-µm finish using diamond suspension. Micro-hardness was performed using an indentation load of 500 g. For each specimen, each hardness data point represents the average of three readings (these hardness indentations were taken centrally 250 µm apart along a horizontal line parallel to the top surface). SEM was performed to study the localized sintering behavior, while making special effort to take images near the hardness indentation, to reveal the representative microstructure. Percent porosity was measured using image analysis, with each data point representing the average of at least three readings. These measurements were conducted (using Imagetool image analysis software) on representative micrographs obtained at magnifications that capture the scale and distribution of porosity. It should be noted that the average depth at which porosity measurements is denoted throughout the article in micrometers also implies $\sim\pm100$ µm vertical span, e.g., 250 µm is 250 ± 100 µm.

Results and discussion

XRD analysis was performed on both the gently rotator mixed (but un-milled) powder and also the 10 h-mechanically alloyed/milled powder. The XRD results for the rotator-mixed powders showed only nickel and aluminum peaks as expected, however, for the mechanically milled powder the Ni and Ti peaks disappeared after 10 h of milling, and amorphous powder was generated. This observed phase development during the MA of our Ni–Ti powder is also in good agreement with previously published study [7, 24, 31]. All CATS experiments were subsequently performed on green compacts of powders mechanically alloyed for 10 h, as explained in the "Experimental procedures" section. The passage of electric current and the corresponding localized heating resulted in the rapid crystallization of the amorphous powder and their simultaneous localized sintering.

Figure 3a shows the development and growth of the process zone under the tip (where local sintering of the powder compact is observed), with an increase in number of duty cycles (i.e., increased cumulative exposure time). It appears that there is a radial expansion of the process zone with the progression of sintering, shifting the sintering front to the surrounding un-sintered regions. Beneath the tip, the central regions displayed the highest densification

at any given distance beneath the surface. Also shown is material depression under the tip after 100 cycles due to local compact shrinkage under the tip. Figure 3b, shows a schematic representation of the proposed process zone evolution using a simplified hemi-spherical geometry for the evolving process zone, assuming a higher resistance surrounding region of un-sintered powder (with high powder–powder contact resistance). It is noted that the evolving sintered region in terms of composition and consolidation, tip and tip/material interfacial properties, together with possible compact cracking under certain conditions should also be considered. However, despite its simplicity, the concept does bring out the idea that the nominal current density assumed at the start of the tip-sintering process (which is simply the applied current divided by the tip/compact contact area) may effectively be reduced as the process zone evolves and grows. Simple calculations show that at a process zone depth of 1 mm, and for a 100-A applied current, the new current density (applied current/surface area of the hemi-spherical process zone) is 1,592 A/cm^2 as opposed to the nominally assumed 12,739 A/cm^2, showing a drastic drop. This could lead to a steady-state size for the process zone when the current density (for a given applied current) drops below some critical value. This is the subject of ongoing study, not only for Ti–Ni but also other material systems as we learn more about this new intriguing process. Here, the specimen thickness can consequently be assumed to play a critical role, in achieving through thickness sintering, processes such as inkjet printing will be investigated for generating thin powder layers.

In both the 70- and 100-cycle CATS materials, the microstructures revealed three distinct phases; dark, medium gray, and a light gray. These were, however, only observed inside the process zone. Similar contrasting phases have previously been reported by numerous authors using different powder-processing routes [25–31, 37], corresponding to $Ti_2Ni/Ti_4Ni_2O_x$, TiNi, and Ni_3Ti, etc. It has previously been reported that $Ti_4Ni_2O_x$ is very difficult to distinguish from Ti_2Ni due to both phases having the same crystal structure and very close lattice parameters [32]. However, a very recent study has shown that interstitial oxygen is soluble in Ti_2Ni and can in fact stabilize the Ti_2Ni phase also at high Ni concentrations [33], thus implying that the phase is actually oxygen-rich Ti_2Ni, i.e., Ti_2Ni (O) (from now on referred to in this article as Ti_2Ni) and not $Ti_4Ni_2O_x$. In the case of Ni–Ti, powders that are amorphized during MA may inherently generate inhomogeneous microstructures despite the intended TiNi base composition, because the TiNi phase was not the most stable in the amorphous state [31]. The small tip-size in CATS is expected to facilitate exceedingly faster sintering, crystallization, and potentially intermetallic phase transformation rates than conventional SPS processing owing to the higher and focused current densities employed. In our present experiments, nominal DC current densities (not pulsed-DC as in conventional SPS) ranging from 6,370 to 12,739 A/cm^2 were investigated. It is noted that these nominal current densities could be further significantly increased by a reduction in tip size, and/or a simple increase in applied current.

Fig. 3 **a** Scanning electron micrographs of the process zone beneath the tip (image is of the central cross section beneath the tip) after 50, 70, and 100 cycles using a current of 100 A. (note that large pores appearing in the sintered regions are in fact material pulled out during the material preparation stage), **b** schematic of progressive resistive layer concept using simplified hemi-spherical process zone model, and **c** SEM image of resistive sintering front/layer for specimen subjected to 30 cycles using a current of 100 A

The small size of our locally sintered/crystallized region precludes the use of XRD for phase analysis; however, energy dispersive X-ray spectroscopy (EDXS) analysis was conducted. Owing to the fine scale of the microstructure and the expected comparatively larger electron beam/material interaction volume, other surrounding phases can contribute to the results of any given targeted region, and hence only a qualitative interpretation of the phase analysis is possible. Nevertheless, the EDXS results do generally approach the compositional categorization of the reported phases, suggesting that the microstructure to consist of Ti_2Ni, TiNi, and Ni_3Ti as previously reported, with the exception that at $\sim$50 μm below the tip/material interface, no NiTi (medium gray phase) could be detected. Considerable amounts of oxygen was also detected even at depths of $\sim$500 μm beneath the tip/material interface (overall on average $\sim$35 at.%). The source of this oxygen may have been from the MA stage, pre-existing oxides on the surface of the as-received powders, and oxygen pick up during CATS due to the possible presence of residual oxygen in the inert argon environment used. Although care was exercised to perform the MA process under an inert argon atmosphere, the presence of some residual oxygen cannot be discounted. Recently, similar levels of oxygen were reported for spark plasma-sintered NiTi "nano" powder which are highly susceptible to oxygen pick up due to their excessive surface area [27]. Only minimal trace of iron was detected due to the use of steel balls and milling vials.

As mentioned, there is no previous study that has investigated the effect of electric current exposure and intensity (or current density) on the evolution of pre-alloyed NiTi powder body/compact during SPS or CATS. Hence, we have proceeded to investigate the evolution of the locally sintered region during CATS, Fig. 4 presents the effect of number of cycles (from 1 to 100, at 100 A) on the micro-hardness, showing an increase in micro-hardness up to a maximum after 70 cycles (i.e., 70 s) followed by a

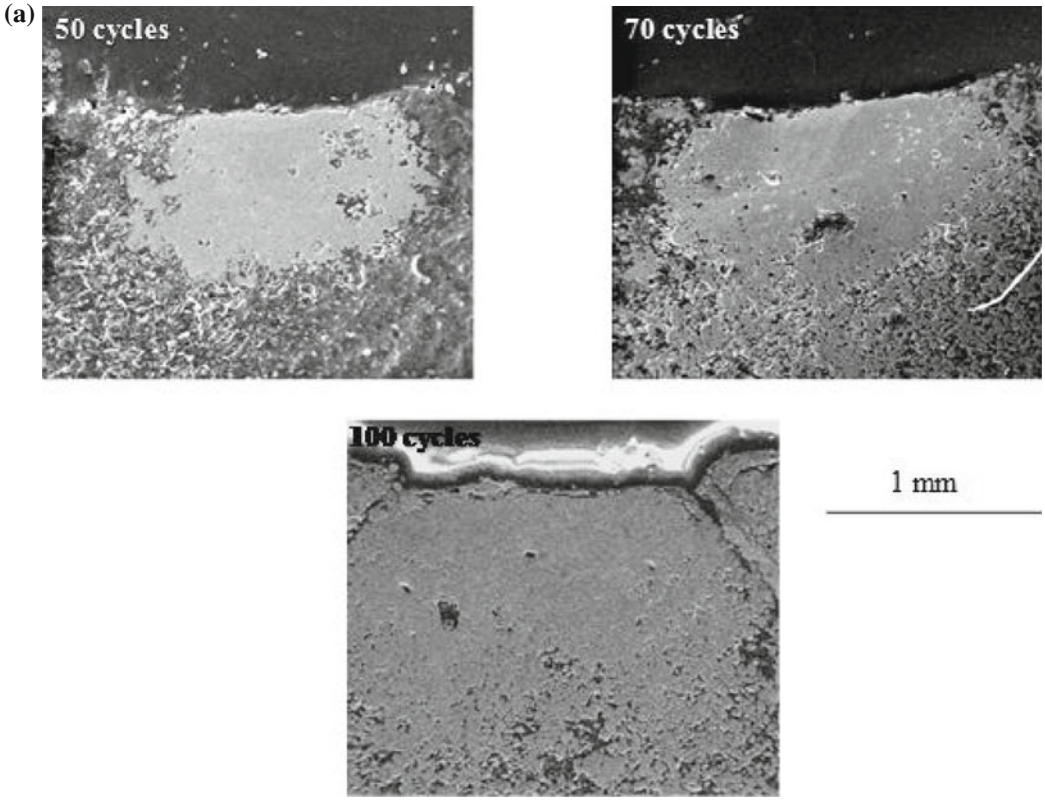
(a)
50 cycles
70 cycles
100 cycles
1 mm

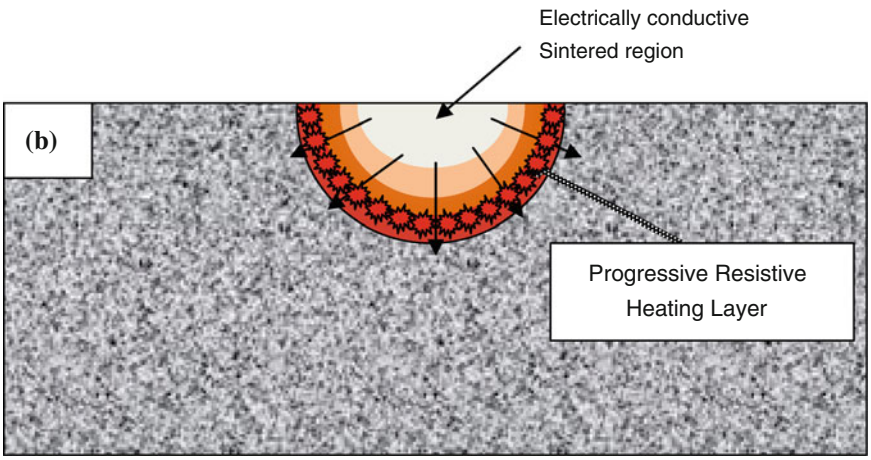
Electrically conductive
Sintered region
(b)
Progressive Resistive
Heating Layer

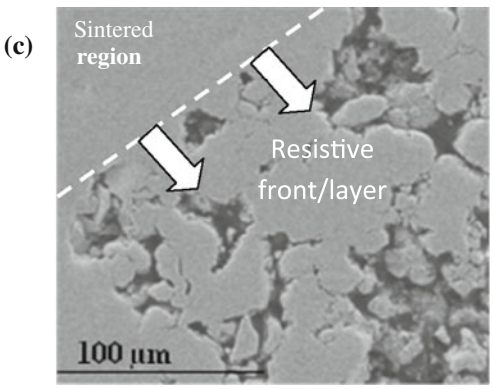
(c)
Sintered
region
Resistive
front/layer
100 µm

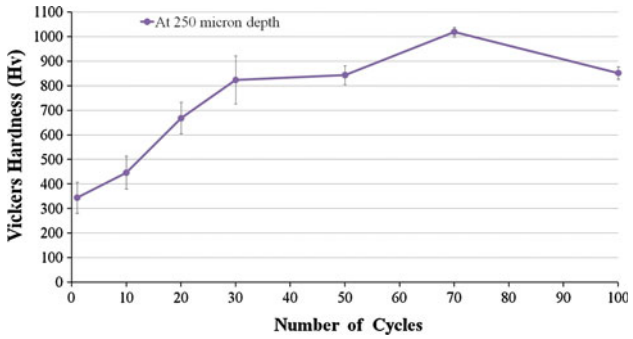

Fig. 4 Effect of number of cycles (at 100 A) on the Vickers micro-hardness (taken at ~250 μm beneath the tip/material interface)

decline at 100 cycles, whereas a continuous decline in porosity was observed to achieve near fully dense material (Fig. 5).

Our refined microstructure can contribute significantly to the observed increased hardness levels. The maximum micro-hardness value for the 70 cycles is primarily due to the reduced levels of porosity and the presence of Ti_2Ni. The decline in micro-hardness at 100 cycles can be explained by considering the volume fraction of Ti_2Ni (dark phase). Figure 6 shows the image analysis results of the apparent percent Ti_2Ni found in the microstructure with increase in number of cycles. All the micrographs were taken at the same magnification, and it may be possible that much smaller nuclei were not detected. It is still interesting though to note the similar decline in amount of Ti_2Ni for the 100 cycle exposure compared to the 70 cycles as also observed in the micro-hardness plot. Ti_2Ni has been reported to be harder than the NiTi phase [34, 35], which in itself depends on whether it is martensitic or austenitic NiTi. As such, the decline in micro-hardness may possibly be explained by a corresponding decline in Ti_2Ni. It is not clear why such a decline in Ti_2Ni occurs, which is the subject of future study. One possible explanation is that the presence of this oxygen-rich phase may affect the local resistivity of the material whereby causing an increase in the local temperature. Interestingly, Ye et al. [31] observed a decline in Ti_2Ni content when the SPS temperature was increased from 900 to 1100 °C. Although they have reported only the data at 10 min of sintering, it still shows a clear effect of temperature. It is highly unfortunate that electric current data is scarce in the large-scale SPS studies on Ni–Ti. Although electric current intensity is a controlled processing parameter in CATS, temperature is not (unlike in the case of SPS); hence isothermal conditions is not investigated with the present CATS setup (study is in progress to add this feature for this novel process, in addition to the ability to perform challenging localized rapid temperature measurements).

Previous study on rapidly quenched amorphous alloys has shown that electric current can in fact enhance the crystallization rate [36]. Moreover, using foil diffusion couples, intermetallic reaction/growth rates have also been reported to be enhanced considerably with electric current intensity/magnitude, for example, in Al–Au and Ni–Ti, and more importantly, the incubation period for phase nucleation has been shown to decrease with increase in current density, such that, at a critical current density, the period has been shown to decrease from many hours to almost zero [13]. Specifically for Ni–Ti, the activation energy for intermetallic phase formation using diffusion couples was found to decline considerably with increase in current (the maximum current density investigated was 2,456 A/cm^2), and the highest intrinsic growth rate constant was that of Ti_2Ni (43×) when using the maximum current density compared with that conducted at the same temperature of 650 °C without current [37]. These studies have contributed considerably to our current understanding; however, unfortunately, no such data are available for powder

Fig. 5 Effect of number of duty cycles (at 100 A) on the % residual porosity

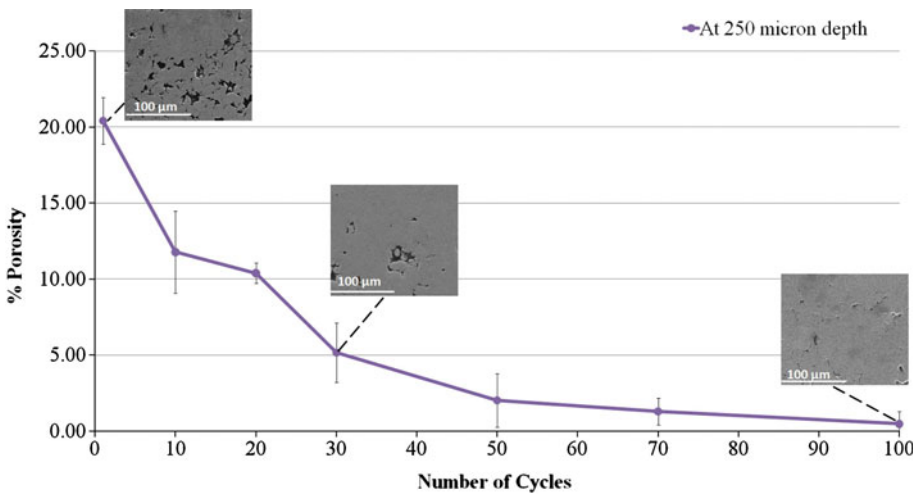

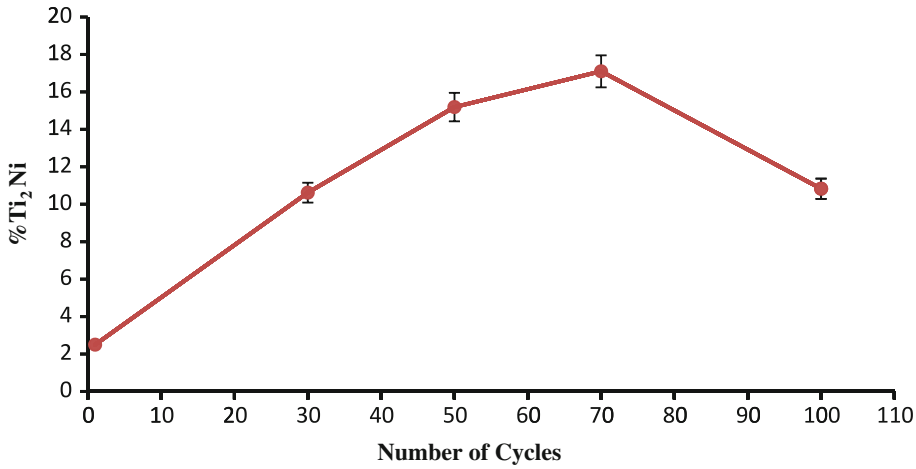

Fig. 6 Effect of number of cycles on Ti_2Ni content

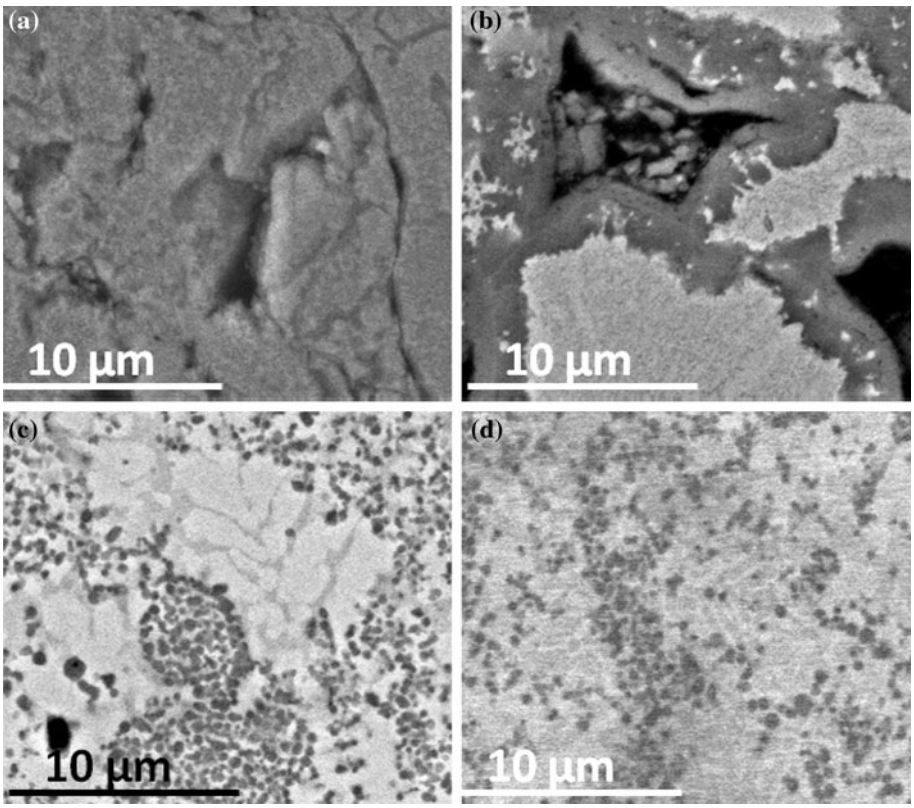

Fig. 7 Scanning electron micrographs of Ni–Ti locally sintered samples after 70 cycles at: **a** 50 A, **b** 70 A, **c** 80 A, and **d** 100 A current intensities, showing pronounced formation of Ti_2Ni at and above 80 A

systems. In our experiments, Fig. 7 shows electron micrographs of the specimen microstructures after 70 cycles of sintering under increasing current intensity. Pronounced Ti_2Ni forms/crystallizes at 80 A and above, with finer Ti_2Ni forming after 70 A (Fig. 8).

Figure 9 shows the effect of increasing electric current intensity on micro-hardness and residual porosity, which is similar to that obtained of increasing number of cycles, i.e., an increase in micro-hardness and a decline in porosity. The fine multi-phase microstructure and porosity similarly contribute to the observed micro-hardness results. Figure 10 shows that at any current level, the degree of sintering decreases with increase in depth below the tip/material interface. Moreover as the current intensity is increased the material at all depths investigated experience increased degrees of sintering.

Figure 11 shows that closer to the compact/tip interface where the highest nominal current density is approached ($\sim$12,739 A/cm^2); full/near full densification is achieved after only 10 s of current exposure. This has been maintained down to even 2 s of current exposure, confirming the positive effects of high current densities. This also underscores the high sensitivity to distance below the tip/material interface. It also suggests that for thin powder (possibly atomized) layers ultra-rapid and through thickness sintering rates should be possible, which is the subject of future study.

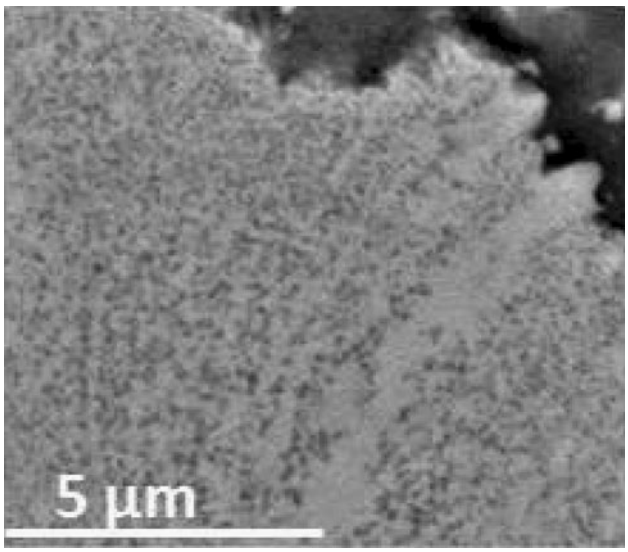

Fig. 8 High magnification electron micrograph showing dark spots (very fine nucleated Ti_2Ni) forming at 70 A after 70 cycles of electric current exposure

Future study will also be directed at investigating the effect of processing atmosphere and conditions on the phase evolution and martensitic transformation temperatures. In addition, CATS in the *moving tip* configuration will be investigated to form NiTi of varying shapes, while also investigating the effect of green density on CATS and its effect on post-processing artifact removal.

Conclusions

The following conclusions can be drawn:

1. Mechanically alloyed Ni/Ti powder was locally sintered to full/near full density for the first time using novel Current Activated Tip-based Sintering in remarkably short times, primarily due to ultra-high current densities employed.
2. The process zone size was found to increase with increased number of cycles (i.e., cumulative current

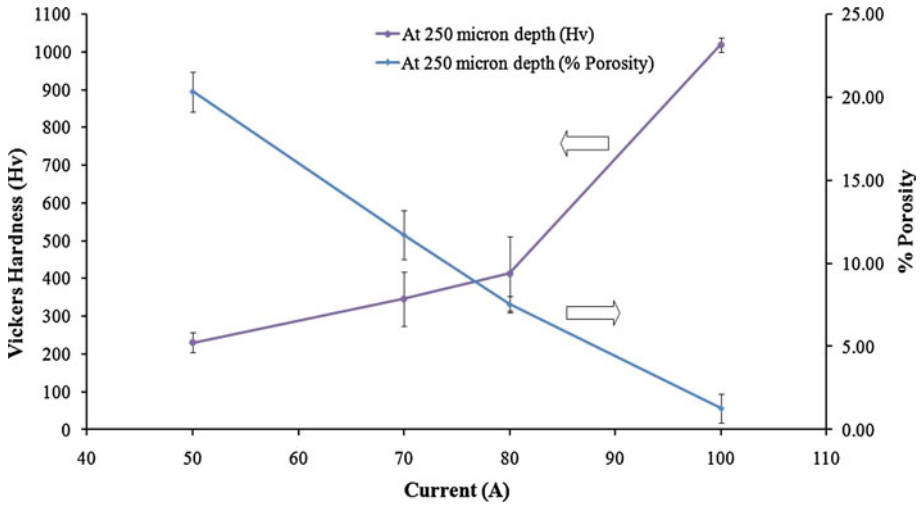

Fig. 9 Vickers micro-hardness (Hv) vs. current intensity (after 70 duty cycles) at 250 µm beneath the tip/material interface

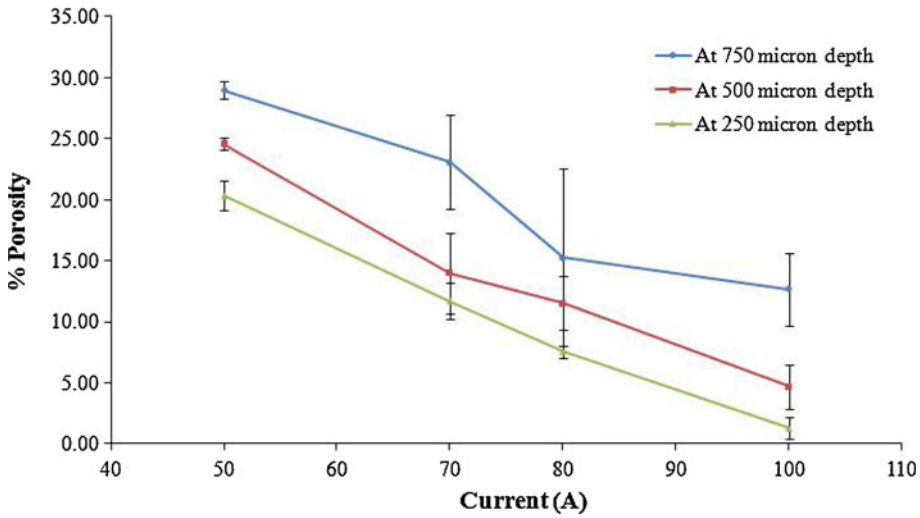

Fig. 10 Effect of current intensity (after 70 duty cycles) on residual porosity levels at varying depths below the tip/material interface

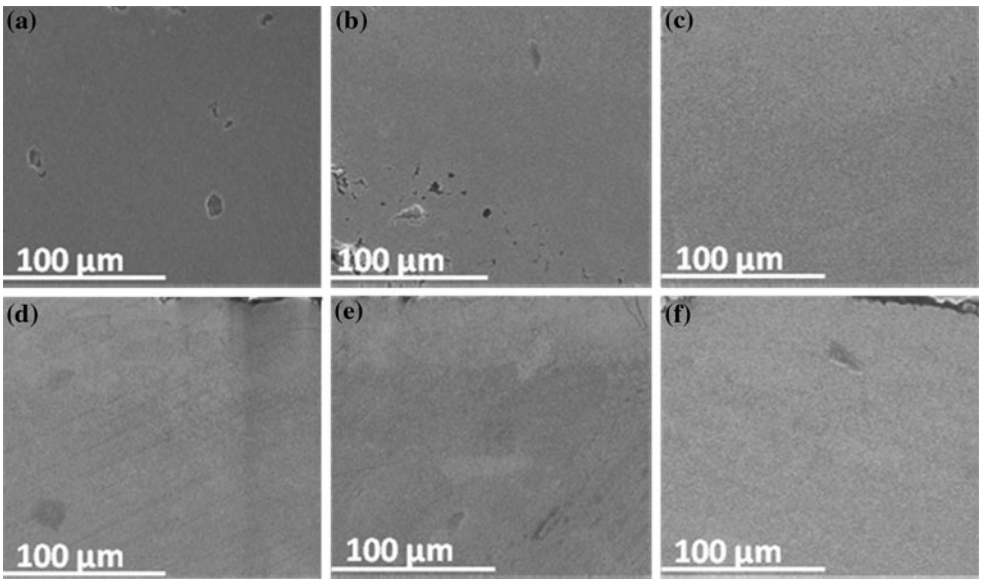

Fig. 11 Regions in immediate proximity to surface exhibiting full/near full densification due to the high nominal current densities: **a** 10, **b** 20, **c** 30, **d** 50, **e** 70, and **f** 100 cycles)

exposure time), suggesting an outer resistive layer is a major contributor to the progressive sintering behavior observed, and analysis suggests a steady-state process zone size under any given applied current, when the effective current density drops below a critical value.

3. The resulting microstructures consisted of multiple phases, suggesting high stability of these phases under the investigated current densities.
4. The effect of increasing current intensity on the Ni/Ti microstructural evolution was investigated for the first time and was found to decrease the residual porosity, and increase hardness.
5. Under 100-A current intensity, micro-hardness was found to increase with number of cycles (exposure time) up to 70 cycles, followed by a decline at 100 cycles, due to a decline in the volume fraction of the harder Ti_2Ni phase. This signifies the important and complex interplay between the electrical properties of phases formed and evolution of the microstructure and properties during CATS.

Acknowledgements The authors express their thanks to Dr. Steve Barlow and Ms. Joan Kimbrough for their help with electron microscopy and XRD. Thanks are also to Mr. Greg Morris and Mr. Mike Lester for general technical support. The authors also wish to thank The National Science Foundation (CMMI division: grant no. 0826532) for their support.

References

1. Jin JL, Chi YH (2002) Mater Sci Forum 394–395:241
2. Zhang L, Xie C, Wu J (2006) Mater Sci Eng A438–440:905
3. Vermaut Ph, Ochin P, Dezellus A, Plaindoux Ph, Dalle F, Muguerra Ph, Portier R (2002) Mater Science Forum 394–395:483
4. Cheng X, Li Z, Xiang G (2007) J Mater Design 28(7):2218
5. Li Z, Xiang G, Cheng X (2006) J Mater Design 27(4):324
6. Hey JC, Jardine AP (1994) Mater Sci Eng A188(1–2):291
7. Takasaki A (1998) Phys Stat Sol A 169:183
8. Schuller E, Krone L, Bram M, Buchkremer HP, Stover D (2004) J Mat-iss.u Werkstofftech 35(5):326
9. Zhang N, Babayan Khosrovabadi P, Lindenhovius JH, Kolster BH (1992) J Mater Sci Eng A150(2):263
10. McNeese MD, Lagoudas DC, Pollock TC (2000) J Mater Sci Eng A 280(2):334
11. Fu YQ, Gu YW, Shearwood C, Luo JK, Flewitt AJ, Milne WI (2006) J Nanotechnology 17(21):5293
12. Morsi K, Patel VV, Moon KS, Garay JE (2008) J Mater Sci 43(12):4050. doi:10.1007/s10853-007-2225-2
13. Munir ZA, Anselmi-Tamburini U (2006) J Mater Sci 41(3):763. doi:10.1007/s10853-006-6555-2
14. Grasso S, Sakka Y, Maizza G (2009) Sci Technol Adv Mater 10:053001
15. Abadie J, Chaillet N, Lexcellent C, Bourjault A (1999) Proc SPIE Int Soc Opt Eng 3667:326
16. Yung KC, Zhu HH (2005) J Smart Mater Struct 14(2):337
17. Schuller E, Krone L, Bram M, Buchkremer HP, Stover D (2005) J Mater Sci 40(16):4231. doi:10.1007/s10853-005-2819-5
18. Morsi K, Moon K, Kassegne S, Ugle R, Villar E (2009) Scripta Mater 60(9):745
19. Morsi K, Moon KS, Current activated tip-based sintering, PCT/US2009/35616 (pending)
20. Locci AM, Orrùb R, Cao G, Munir ZA (2003) Intermetallics 11:555
21. Koch CC (1989) Ann Rev Mater Sci 19:121
22. Suryanarayana C (2001) Prog Mater Sci 46:1
23. Chen W, Anselmi-Tamburini U, Garay JE, Groza JR, Munir ZA (2005) Mater Sci Eng A394:1332
24. Zoz H, Ernst D, Ahn IS, Kwon WH (1997) In: Ward-Close CM, Froes FH, Cho SS, Chellman DJ (eds) Synthesis/processing of lightweight metallic materials. TMS, Warrendale

25. Otsuka K, Wayman CM (1988) Shape memory materials. Cambridge University Press, Cambridge
26. Bertheville B, Bidaux J-E (2005) Scripta Mater 52:507
27. Shearwood C, Fu YQ, Yu L, Khor KA (2005) Scripta Mater 52:455
28. Schuller E, Bram M, Buchkremer HP, Stover D (2004) Mater Sci Eng A378:165
29. Bram M, Ahmad-Khanlou A, Heckmann A, Fuchs B, Buchkremer HP, Stover D (2002) Mater Sci Eng A337:254
30. Krone L, Schuller E, Bram M, Hamed O, Buschkremer H-P, Stover D (2004) Mater Sci Eng A378:185
31. Ye LL, Liu ZG, Raviprasad K, Quan MX, Umemoto M, Hu ZQ (1998) Mater Sci Eng A241:290
32. Luo H, Shan F, Huo Y, Wang Y (1999) Thin Solid Films 339:305
33. Frenzel J, George EP, Dlouhy A, Somsen Ch, Wagner MF-X, Eggeler G (2010) Acta Mater 58:3444
34. Hiraga H, Inoue T, Shimura H, Matsunawa A (1999) Wear 231:272
35. Tan L, Crone WC (2002) Acta Mater 50:4449
36. Conrad H (2002) Mater Sci Eng A287:227
37. Garay JE, Anselmi-Tamburini U, Munir ZA (2003) Acta Mater 51(15):4487